A Method for the Design of Compliant Mechanisms With Small-Length Flexural Pivots

L. L. Howell
Graduate Research Assistant.

A. Midha
Professor.

Elastic Mechanisms Laboratory,
School of Mechanical Engineering,
Purdue University,
West Lafayette, IN 47907

Compliant or flexible-link mechanisms gain some or all of their motion from the relative flexibility of their joints rather than from rigid-body joints only. Unlike rigid-body mechanisms, energy is not conserved between the input and output ports of compliant mechanisms because of energy storage in the flexible members. This effect and the nonlinearities introduced by large deflections complicate the analysis of such mechanisms. The design of compliant mechanisms in industry is currently accomplished by expensive trial and error methods. This paper introduces a method to aid in the design of a class of compliant mechanisms wherein the flexible sections (flexural pivots) are small in length compared to the relatively rigid sections. The method includes a definition and use of a pseudo-rigid-body model, and the use of a large-deflection finite element type algorithm. An example is used to illustrate the design technique described.

Introduction

There is a relatively unknown and unexplored branch of mechanisms called compliant or flexible-link mechanisms. Such mechanisms gain mobility from the relative flexibility of their members rather than from rigid-body joints only. Figure 1 shows two examples of compliant mechanisms (Salamon, 1989). Both mechanisms would be classified as structures in classical rigid-body kinematics, but the ability of some members to flex gives them mobility, and the ability to perform useful work. The challenge presented by such mechanisms is that energy is no longer conserved between their input and output ports because of energy storage in the flexible members. This effect coupled with the nonlinearities introduced by large deflections of flexing members complicates the analysis. Due to these difficulties, the design of compliant mechanisms in industry is currently accomplished by expensive trial and error methods.

Though the analysis is involved, there are advantages to compliant mechanisms. One of these is that a mechanism can be built in one piece, if manufactured from an extrudable or injection-moldable material. This not only simplifies manufacturing, but can also reduce weight and eliminate wear, backlash, noise, and need for lubrication (Sevak and McLarnan, 1974; Her, 1986; Salamon, 1989).

As stated, compliant mechanisms gain at least some of their motion from the deflections of their flexible members. For many simple mechanisms, these deflections are small and conventional linear beam theory may be used in the deflection and motion analysis. Often, however, the deflections are relatively large and the small-deflection assumptions used to linearize the beam equations are no longer valid. The difference in analysis lies in the treatment of the Bernoulli-Euler beam equation, which states that the bending moment is proportional to beam curvature. Using the exact equation for curvature the beam equation can be written as

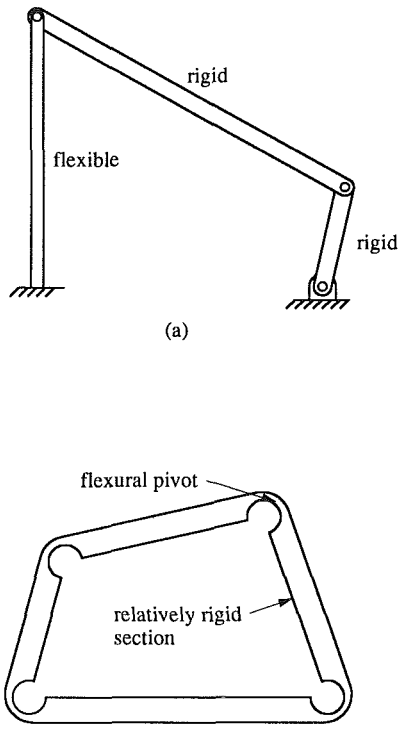

Fig. 1 *(a)* **A partially compliant and** *(b)* **a fully compliant mechanism**

Contributed by the Mechanisms Committee for publication in the JOURNAL OF MECHANICAL DESIGN. Manuscript received April 1992. Associate Technical Editor: B. J. Thompson.

$$M = EI\frac{d\theta}{ds} = EI\frac{\dfrac{d^2y}{dx^2}}{\left(1+\left(\dfrac{dy}{dx}\right)^2\right)^{3/2}} \quad (1)$$

where M is the moment, $d\theta/ds$ the rate of change in angular deflection along the beam (curvature), y the transverse deflection, x the coordinate along the undeflected beam axis, and EI the flexural rigidity. For small deflections, the square of the slope $(dy/dx)^2$ can be assumed to be small compared to unity, and the denominator in Eq. (1) may be ignored. The curvature may then be approximated by the second derivative of y, i.e., d^2y/dx^2. This linearization leads to the classical beam moment-curvature equation

$$M = EI\frac{d^2y}{dx^2} \quad (2)$$

The assumption described above cannot be used in the analysis of large deflections since the slope of the transverse deflection is no longer small. There are several methods available that take into account the nonlinearities introduced by large deflections. One method used to find a closed-form solution involves the solution of a second-order, nonlinear differential equation using elliptic integrals (Bisshopp and Drucker, 1945; Frisch-Fay, 1969; Gorski, 1976). The advantage of this solution technique is that it provides exact, closed-form solutions. The disadvantage is that the derivations are cumbersome and solutions only exist for relatively simple geometries and loadings.

Several numerical techniques have been explored and suggested for use in large-deflection analysis. Several large-deflection finite element techniques are available and offer a versatile approach for solving general problems (Bathe, 1979; Yang, 1986; Zienkiewicz, 1989). The disadvantage of conventional large-deflection finite element analysis is the computation time involved in the solution. A similar technique uses the same basic theory as finite elements, but employs a different method to obtain the solution of the resulting equations. This technique, called the chain algorithm, reduces the computation time dramatically for certain types of problems. An explanation of the algorithm's use in compliant mechanisms will be discussed and a more in-depth explanation with mathematical details is given in the Appendix, and Midha et al. (1992).

Various researchers have added valuable insights into other areas of compliant mechanism analysis and design. Shoup and McLarnan (1971) and Shoup (1972) used the equations of the undulating and nodal elastica for the analysis of flexible-link mechanisms. The resulting method requires the solution of a set of nonlinear equations involving elliptic integrals of the first and second kind. Design charts were developed to help determine good initial guesses for the iterative solution technique used to solve the system of equations. Winter and Shoup (1972) used similar equations to generate coupler curves for a partially compliant mechanism, similar to that shown in Fig. 1(*a*). Sevak and McLarnan (1974) coupled a finite element method with an optimization technique to synthesize a flexible-link mechanism for function generation. Fletcher and Powell's variable metric method was used to minimize the unconstrained error function for mechanisms in which one or two links were flexible. Her (1986), Hill (1987), and Salamon (1989) used a finite element type chain algorithm to aid in the analysis and design of compliant mechanisms. Salamon also proposed a general design methodology which included synthesizing a rigid-body mechanism first, selectively introducing compliance to obtain a pseudo-rigid-body mechanism, and finally obtaining and analyzing a fully compliant model. This methodology is the progenitor of the design method described in this work.

In general, obtaining an accurate pseudo-rigid-body model for an arbitrary compliant mechanism would be a difficult task because its kinematic inversions may yield many more mechanisms than those of a rigid-body counterpart. These difficulties have been addressed in works by Burns and Crossley 1966), Shoup and McLarnen (1971), Her (1986), and Her and Midha (1987). The current discussion, however, is centered around compliant mechanisms with small flexural segments compared to the rigid sections. Such an arrangement results in obvious choices for the location of the pseudo-rigid-body joints, and thus an approximate pseudo-rigid-body model is readily obtained.

Introduced herein is a computer-aided design approach which uses rigid-body kinematic analysis and large-deflection analysis via a finite element type algorithm, as tools for the design of a class of compliant mechanisms. The method is applicable for mechanisms comprised of flexible segments (flexural pivots) that are considerably smaller than the lengths of the more rigid sections. The reason for this distinction will be discussed in the next section.

The method discussed is exemplified with the design of a compliant mechanism. This example mechanism is a hand tool which needs to be designed for high mechanical advantage, be made of one piece, and have geometry and motion similar to a classical rigid-body four-bar mechanism. That is, it should have four flexural pivots (relatively flexible sections) and four relatively rigid sections connected in a closed loop, such as the mechanism shown in Fig. 1(*b*).

Design and Analysis

Salamon (1989) proposed a general design method for compliant mechanisms. Figure 2 shows this method in a slightly revised form (conditional blocks have been added). In this method, rigid-body and pseudo-rigid-body mechanisms are generated. A pseudo-rigid-body mechanism models flexible members as discrete springs attached to rigid links, where the rigid links represent the more rigid segments of the compliant mechanism. The pseudo-rigid-body mechanism is analyzed to see if the design specifications and constraints are satisfied. If they are not met, the pseudo-rigid-body mechanism may be modified and analyzed again. The loop involving the modi-

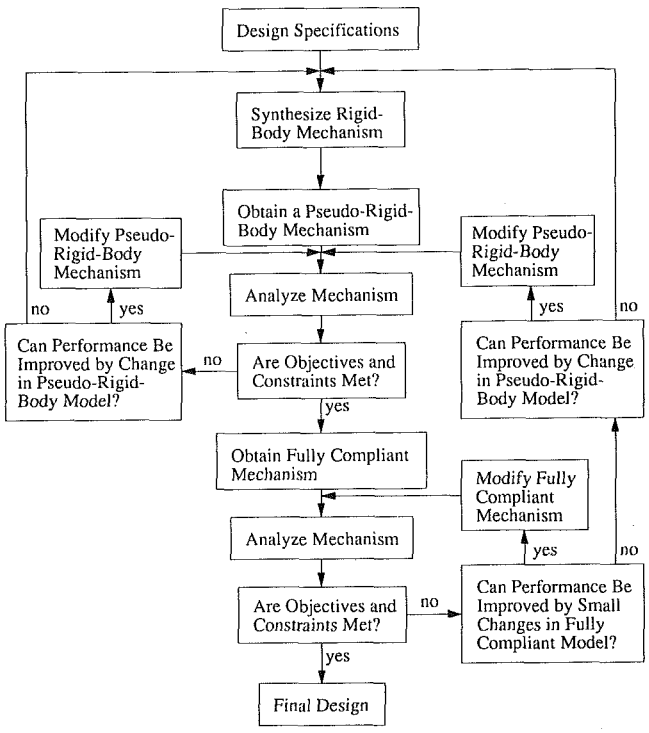

Fig. 2 Flow chart for a compliant mechanism design process

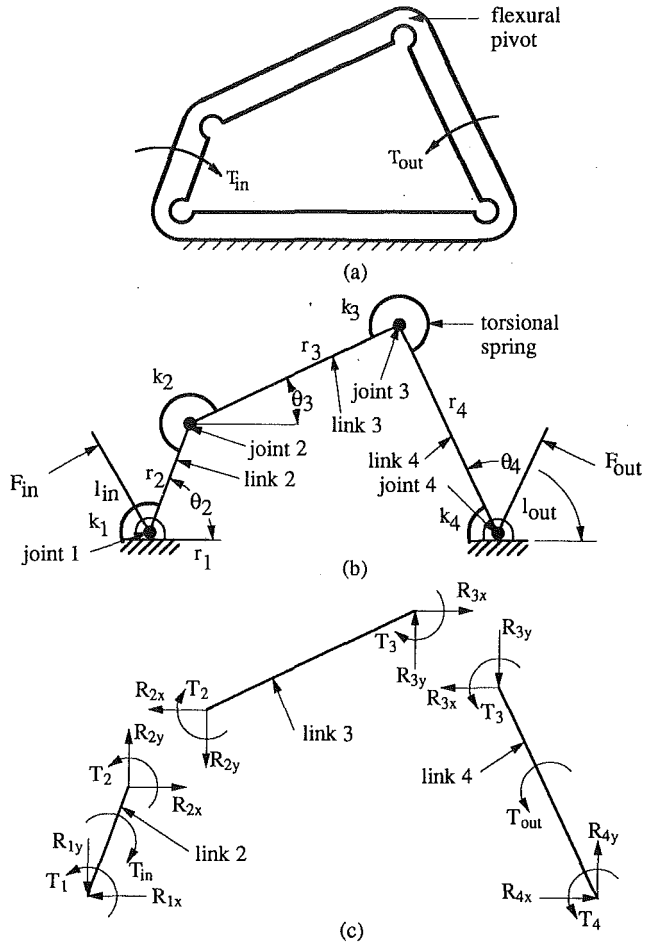

Fig. 3 *(a)* **A compliant mechanism,** *(b)* **its pseudo-rigid-body model, and** *(c)* **free-body diagrams for moving links**

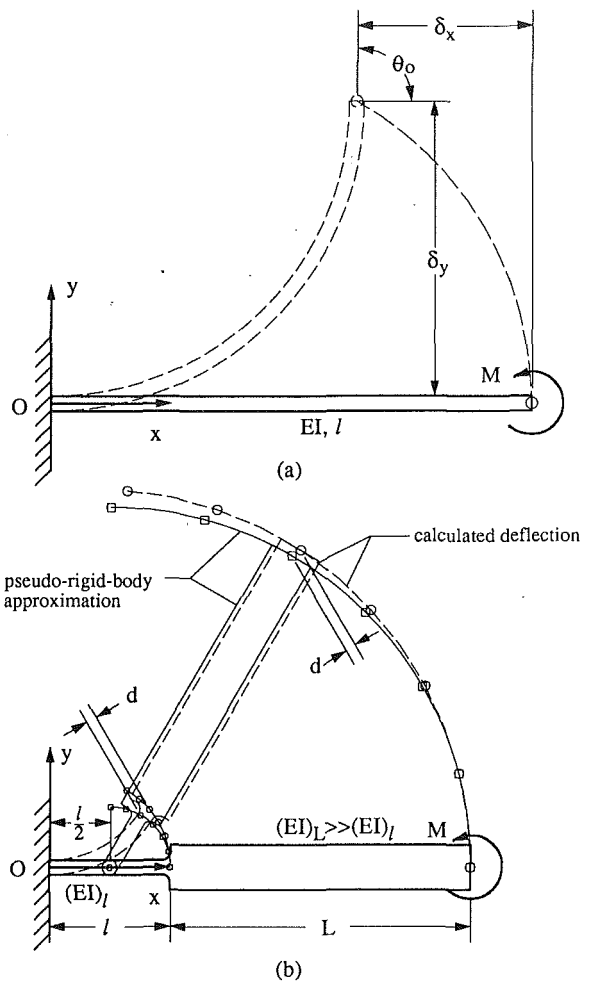

Fig. 4 *(a)* **Large deflection of a flexible beam with an end moment, and** *(b)* **a pseudo-rigid-body approximation**

fication and analysis of the pseudo-rigid-body mechanism may be a simple iterative method or a formal optimization routine. The designer may occasionally find that the design objectives are not readily satisfied with the type of mechanism chosen. In this case it is necessary to design a new rigid-body mechanism and start the process again.

Once an appropriate pseudo-rigid-body mechanism is found, the model is used to obtain a fully compliant mechanism. The fully compliant model is analyzed by means of a large-deflection analysis method. If the pseudo-rigid-body model was accurate, this step may simply serve as a means to verify that the objectives have been met, and to analyze the mechanism performance. Small design changes to improve performance may be made by modifying the compliant model. If analysis reveals that large adjustments are necessary, the pseudo-rigid-body model or the initial rigid-body mechanism may be modified.

The discussion here will focus primarily on three major areas: pseudo-rigid-body mechanism analysis, modification of pseudo-rigid-body model, and fully compliant mechanism analysis.

Initial Pseudo-Rigid-Body Analysis. There is currently very little known about the analysis of compliant mechanisms. It would, therefore, be of value to model these mechanisms in a manner such that knowledge of rigid-body kinematics may be used for guidance in design. The idea of a pseudo-rigid-body model was developed with this in mind. An example of a pseudo-rigid-body model is shown in Fig. 3. Here, the flexural pivots [the relatively more flexible sections in the compliant mechanism in Fig. 3(*a*)] are modeled as torsional springs attached to the rigid-body joints in Fig. 3(*b*).

In order to use such a model, some simplifying assumptions must be made. First, it is assumed that the motion of the compliant mechanism resembles that of the pseudo-rigid-body mechanism. This assumption will tend to be more accurate as the lengths of the flexural pivots [Fig. 3(*a*)] decrease compared to those of the relatively rigid sections. This may be illustrated by the uniform cross-section beam in Fig. 4(*a*). For a pure end moment, M, the Bernoulli-Euler equation is expressed (Shigley and Mischke, 1989) as

$$\frac{d\theta}{ds} = \frac{M}{EI} \tag{3}$$

Separating variables and integrating:

$$\int_0^{\theta_0} d\theta = \frac{M}{EI} \int_0^{l} ds \tag{4}$$

$$\theta_o = \frac{Ml}{EI} \tag{5}$$

The vertical deflection may be found by writing the curvature as

$$\frac{d\theta}{ds} = \frac{d\theta}{dy}\frac{dy}{ds} = \frac{d\theta}{dy}\sin\theta \tag{6a}$$

and for the horizontal deflection

$$\frac{d\theta}{ds} = \frac{d\theta}{dx}\frac{dx}{ds} = \frac{d\theta}{dx}\cos\theta \tag{6b}$$

Combining Eqs. (3), (5), and (6*a*) and separating variables yields:

$$\frac{1}{l}\int_0^{\delta_y} dy = \frac{1}{\theta_o}\int_0^{\theta_o} \sin\theta d\theta \tag{7}$$

$$\frac{\delta_y}{l} = \frac{1-\cos\theta_o}{\theta_o} \tag{8}$$

The same procedure is followed to find the horizontal deflection, resulting in

$$\frac{l-\delta_x}{l} = \frac{\sin\theta_o}{\theta_o} \tag{9}$$

Figure 4(*a*) shows this deflection path for a beam of constant flexural rigidity, *EI*. These results may be used as a simple illustration of the comparative accuracy of the pseudo-rigid-body approximations.

Figure 4(*b*) shows a beam with a flexible section of length l and flexural rigidity $(EI)_l$, connected to a rigid section of length L and rigidity $(EI)_L$, where $(EI)_L \gg (EI)_l$. The deflection of the beam is calculated from Eqs. (8) and (9) above, and the deflected configuration is shown in dashed lines. This path is also approximated by two rigid links connected by a revolute joint at $l/2$, and the displacement path is shown in solid lines. For a given angular deflection, the rigid sections of the calculated and approximated beams will be parallel, causing the distance between the corresponding path points determined by the two methods, d, to be the same at both ends of the rigid section, as shown in Fig. 4(*b*). This distance, d, will obviously decrease with decreasing l. For this reason, the accuracy of the pseudo-rigid-body model shown in Fig. 3 is improved by insuring that the lengths of the flexural pivots are small compared to the lengths of the rigid sections. Similar results can be shown for other end loads.

It is also assumed that the bending stiffness of a pivot approximates its torsional spring stiffness. The initial estimate used for the spring stiffness is obtained form elementary beam theory (Shigley and Mischke, 1989):

$$k = \frac{EI}{l} \tag{10}$$

where E is the modulus of elasticity, I the cross-sectional moment of inertia and l the pivot length. This assumption will be more accurate if bending is the more dominant loading in the flexural pivot. Since this stiffness is assumed to be that of a beam under pure bending, the model essentially neglects the transverse and axial loads applied to the pivots. Therefore, as these loads grow larger compared to the bending moment, greater error will be introduced to the model. An advantage of this simple model is that for pure bending, the equation $M = EI/l\,\theta$ is accurate even for large-deflections, since no small-deflection linearizations have been made. The errors introduced by this model will be accounted for in the fully compliant mechanism analysis discussed later in this paper.

Materials with nonlinear stress-strain characteristics may also be modeled by approximating a linear modulus over the appropriate range of deflections and strains. If the nonlinearity is large for the above approximation to be accurate, a nonlinear form for the spring constant in Eq. (10) may be defined.

The pseudo-rigid-body model may be analyzed by constructing a free-body diagram for each link, as shown in Fig. 3(*c*). The torque at each joint caused by the deflection of the torsional springs may be written as

$$\begin{aligned} T_1 &= k_1(\theta_{2s}-\theta_2) \\ T_2 &= k_2(\theta_3-\theta_{3s}+\theta_{2s}-\theta_2) \\ T_3 &= k_3(\theta_{4s}-\theta_4+\theta_3-\theta_{3s}) \\ T_4 &= k_4(\theta_{4s}-\theta_4) \end{aligned} \tag{11}$$

where T_i is the torque caused by torsional spring i, with spring constant k_i, and θ_{is} represents the (starting) value of θ_i at which the spring is unstrained.

The equations of static equilibrium may be used to solve for the unknown reactions and output torque in Fig. 3(*c*). Summing the forces in the x and y directions and rearranging we find

$$\begin{aligned} R_x &= R_{1x} = R_{2x} = R_{3x} = R_{4x} \\ R_y &= R_{1y} = R_{2y} = R_{3y} = R_{4y} \end{aligned} \tag{12}$$

where the reactions are defined in Fig. 3(*c*). Summing the moments for each link yields:

$$\begin{aligned} T_2 + T_3 + R_x r_3 \sin\theta_3 - R_y r_3 \cos\theta_3 &= 0 \\ T_3 + T_{out} + T_4 + R_x r_4 \sin\theta_4 - R_y r_4 \cos\theta_4 &= 0 \\ T_1 - T_{in} + T_2 + R_x r_2 \sin\theta_2 - R_y r_2 \cos\theta_2 &= 0 \end{aligned} \tag{13}$$

Assuming that the input torque, T_{in}, is known, the three equations can be solved algebraically for the three unknowns, R_x, R_y, and T_{out}, where T_{out} is the output torque. This results in

$$T_{out} = B + Ch_2 - Ah_3 \tag{14}$$

where h_i is the coefficient $d\theta_i/d\theta_4$. These coefficients are determined from kinematics (Paul, 1979) as:

$$\begin{aligned} h_2 &= \frac{r_4 \sin(\theta_3-\theta_4)}{r_2 \sin(\theta_3-\theta_2)} \\ h_3 &= \frac{r_4 \sin(\theta_4-\theta_2)}{r_3 \sin(\theta_3-\theta_2)} \end{aligned} \tag{15}$$

The coefficients A, B, and C for the mechanism in Fig. 3 are found to be

$$\begin{aligned} A &= -T_2 - T_3 \\ B &= -T_4 - T_3 \\ C &= -T_1 - T_2 + T_{in} \end{aligned} \tag{16}$$

The pseudo-rigid-body model for the compliant hand tool in Fig. 5(*a*) [and its compliant counterpart in Fig. 5(*b*)] would differ from the mechanism in Fig. 3 in that the input is applied to link 3 rather than link 2. This means that the input moment arm, l_{in}, is the shortest distance from the input force, F_{in}, to the relative instant center I_{13} (Erdman and Sandor, 1984). The instant center represents a point where there is no relative velocity between two links at a given instant. Instant center I_{13} for links 1 and 3 is found as shown in Fig. 5(*a*). With this in mind, the output torque equation for the hand tool model remains the same as Eq. (14), except the coefficients A, B, and C now become

$$\begin{aligned} A &= -T_2 - T_3 + T_{in} \\ B &= -T_4 - T_3 \\ C &= -T_1 - T_2 \end{aligned} \tag{17}$$

This type of model is instrumental in ascertaining the mechanism type ("four-bar" mechanism, etc.) to be used, and the approximate lengths and orientations of the "rigid links." In the design of the compliant hand tool, for example, the general configuration type chose is shown in Fig. 5(*a*). It was also discovered that when a link is always in compression, one pivot could readily be replaced by a "passive" pivot (Salamon, 1989), as shown in Fig. 5(*c*). A passive pivot transmits compressive loads while serving as a bearing between two contacting surfaces. The energy lost to friction is assumed to be small compared to the energy storage in active flexural pivots.

Modification of Pseudo-Rigid-Body Model to Improve Performance. With the basic configuration of the mechanism determined, the pseudo-rigid-body model can be analyzed and modified to improve mechanism performance. The modifi-

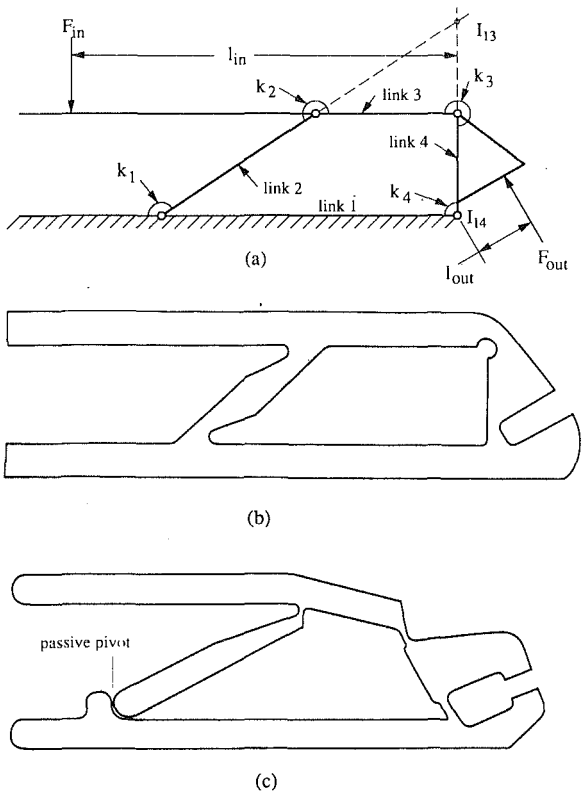

Fig. 5 (*a*) Pseudo-rigid-body model for hand-tool, (*b*) its compliant counterpart, and (*c*) the design after pseudo-rigid-body analysis

cations may be accomplished by either trial and error or by means of formal optimization techniques. The first step is to determine the objective function, or what aspect of the design is to be improved. For instance, when high mechanical advantage is desired, the objective function may be written to assist in determining the maximum output force for a given input force and link configuration. The error function or structural error (Erdman and Sandor,1984) can be minimized for function or path generation problems, respectively. Possible design variables include the lengths and thicknesses of the pivots, lengths of the rigid sections, initial link orientations and width of the mechanism. Potential constraints include stress limits, buckling of compression members, min/max thickness and length of pivots and rigid sections, mobility requirements, maximum structural error and min/max input force. Such problems may be solved by nonlinear optimization methods such as the augmented Lagrangian (Vanderplaats, 1984) or internal penalty function (Rao, 1984) methods. Further design studies may then be carried out by varying parameters such as modulus of elasticity, yield strength and range of motion.

In the design of the compliant hand tool, the thickness and length of the three active pivots are the design variables. Design studies are also carried out by varying the "rigid link" lengths and orientations to find the best design; so these may also be considered as design variables. The lengths of the more rigid sections and their initial orientations contribute significantly to the mechanism performance. The initial orientation of links may be especially vital in toggle mechanisms, such as the hand tool, which gain their high mechanical advantage by operating near the toggle position.

The toggle position describes the mechanism orientation when links 2 and 3 in Fig. 5(*a*) [or the corresponding rigid sections of the compliant mechanism in Fig. 5(*c*)] are collinear. For a rigid-link mechanism with no springs, Eqs. (14) and (17) give $T_{out} = -T_{in}h_3$, where h_3 is defined in Eqs. (15). The mechanical advantage (ma) is given as

$$ma = \frac{F_{out}}{F_{in}} = -\frac{l_{in}}{l_{out}} h_3 \tag{18}$$

since $T_{in} = F_{in}l_{in}$ and $T_{out} = F_{out}l_{out}$ [Fig. 5(*a*)]. Examination of the coefficient h_3 in Eqs. (15) reveals that this term tends to infinity as the mechanism approaches toggle ($\theta_2 = \theta_3$), and the mechanical advantage increases dramatically. For compliant mechanism, this may be used to counter the effects of energy storage in the flexural pivots. This will be demonstrated in the analysis of the compliant hand tool.

The original lengths of the rigid sections were chosen in light of the preceding discussion of rigid-body toggle mechanisms. Note the similarity in link length ratios between the compliant hand tool and, say, the commercially available Peterson's vice grips. The choice of initial orientation of these segments, however, is not as straightforward. The mechanism must start out close enough to the toggle position such that an appropriate mechanical advantage will result (*i*) for a workpiece that just fits in the grips, and (*ii*) for smaller workpieces as well. The orientations should be chosen carefully since much energy can be lost to storage in the pivots if the mechanism must undergo large deflections before reaching the workpiece (Salamon, 1989). Much of the energy storage problem could be solved by using adjustable grips for different sized workpieces.

The performance of the hand tool will depend largely on its ability to have a large mechanical advantage while not exceeding stress limits. Therefore, it is important to maximize the output force (torque) for a given input force (torque). With this in mind, the objective function for the pseudo-rigid-body model is expressed by Eq. (14):

$$T_{out} = B + Ch_2 - Ah_3 \tag{14}$$

where T_{out} is the output torque to be maximized and the other parameters are as defined in Eqs. (10), (11), (15), and (17). Stress constraints for the active flexural pivots are expressed as

$$\sigma_i < \frac{S_y}{(FS)_i}; \quad i = 2,3,4 \tag{19}$$

where

$$\sigma_i = \left|\frac{F_i}{wt_i}\right| + \left|\frac{Et_i\Delta\theta_i}{2l_i}\right| \tag{20}$$

and σ_i, $(FS)_i$, t_i, l_i, and F_i are the normal stress, factor of safety, thickness, length, and axial force corresponding to pivot i, and S_y, E and w are the material yield strength, modulus of elasticity and width, respectively, and $\Delta\theta_i$ is the angle of deflection in the motion of pivot i. Other constraints include the minimum thickness of flexural pivots due to manufacturing constraints, and the maximum length of the pivots, to ensure that the pivot lengths remain much smaller than the lengths of the rigid sections. These are expressed as:

$$\begin{aligned} 0.01 \le t_i \le 0.375 \\ 0.01 \le l_i \le 0.375 \end{aligned} \tag{21}$$

The discussion above may be summarized as follows:

Find the design vector (vector of design variables)

$$\mathbf{X} = \begin{Bmatrix} t_2 \\ t_3 \\ t_4 \\ l_2 \\ l_3 \\ l_4 \end{Bmatrix}$$

which maximizes the objective function

$$T_{out}(\mathbf{X}) = B(\mathbf{X}) + C(\mathbf{X})h_2 - A(\mathbf{X})h_3 \tag{22}$$

subject to the constraints

$$g_j(\mathbf{X}) = \sigma_i < \frac{S_y}{(FS)_i}; \quad i = 2,3,4; \quad j = 1,2,3$$

$$g_j(\mathbf{X}) = t_i \leq .375; \quad i = 2,3,4; \quad j = 4,5,6$$

$$g_j(\mathbf{X}) = t_i \geq .01; \quad i = 2,3,4; \quad j = 7,8,9$$

$$g_j(\mathbf{X}) = l_i \leq .375; \quad i = 2,3,4; \quad j = 10,11,12$$

$$g_j(\mathbf{X}) = l_i \geq .010; \quad i = 2,3,4; \quad j = 13,14,15$$

The resulting mechanism is shown in Fig. 5(*c*).

Several important ideas evolve from this work. In the hand tool design, for instance, it was discovered that the ideal material for pivots is one with a high strength to modulus of elasticity ratio. From Eq. (5), for a specific θ_o, L and I, the moment required to deflect the pivot will decrease with decreasing E. Therefore, a pivot in bending with known angular deflection requirements and geometry will more easily be within the stress constraints for a higher material strength to modulus of elasticity ratio. It was also discovered that the mechanism performance could be improved by moving the passive pivot [Fig. 5(*c*)] to the upper joint of link 2, since it bends through a much larger angle of deflection. This change and others will be further illustrated later.

Calculations are performed assuming the mechanism to be .685-in. wide, made from Delrin, an Acetal-based Dupont product with a yield strength of 10,000 psi, and a factor of safety (*F.S.*) of 1.5. The modulus of elasticity is approximated as constant with an experimentally determined value of 300,000 psi.

Analysis of Fully Compliant Model. A pseudo-rigid-body model is very useful in determining the general lengths of pivots and links and their orientations, but a more accurate method is required to further improve the design and perform the final analysis. The final data obtained from the pseudo-rigid-body design phase is taken and analyzed using the methods described below.

Chain Algorithm. In the fully compliant model, a finite element type procedure employing a chain algorithm is used (Her, 1986). A brief explanation of the algorithm is given here and a more in-depth description and mathematical details are included in the Appendix, and Midha et al. (1992). The chain algorithm is so named because it discretizes the object being modeled into beam elements and analyzes each element in succession. Figure 6 shows a general flexible member to be analyzed. The chain algorithm begins calculations at element 1 by assuming that node 0 is fixed. The equivalent external loads at node 1 are then determined by finding the internal loads at that node by using the equations of static equilibrium. The deflections of this element are now found as if it were a single cantilever beam. As the algorithm continues, it moves the next elements through a rigid-body rotation such that the angles are compatible at the end of element 1 and the beginning of element 2. Equivalent loads are now found for element 2 at node 2, and it is analyzed again as a single cantilever beam (Fig. 6). When the deflections are found, the following elements are rotated and translated such that the angles at node 2 are compatible. The sequence of finding equivalent end loads, calculating deflections, and rotating remaining elements is repeated for each element until the last element is reached. Accuracy and stability are helped by two factors. First, it is important that the discretization be fine in areas of large deflection. Second, the load should be added in increments such that improved estimates of moment arms can be found for the equivalent end load calculations.

Shooting Method. The chain algorithm calculates the deflection of a flexible member fixed at one end. A shooting method may be used in conjunction with the chain algorithm when additional boundary conditions must be met. These

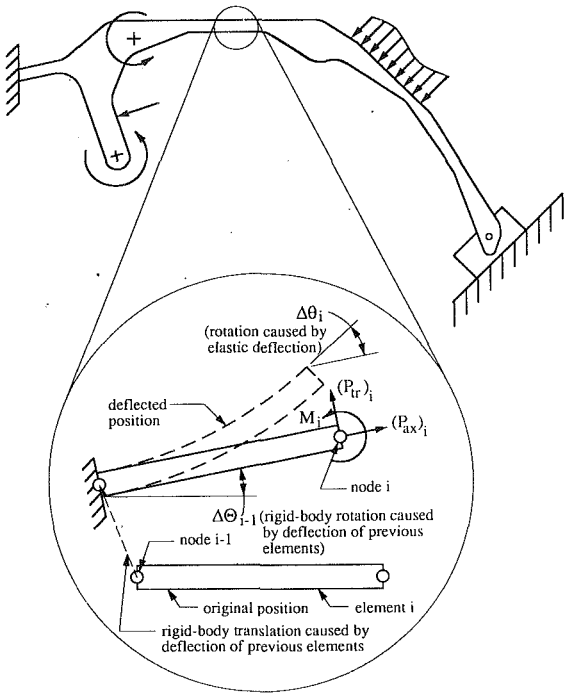

Fig. 6 A generalized compliant mechanism and a typical beam element as used by the chain algorithm

boundary conditions are generally position and rotation constraints at a finite number of nodes. For example, consider the slider in Fig. 7. The boundary conditions for this mechanism would be no rotation and no vertical deflection at the slider, and no translations and no rotation at the fixed end. Since the chain algorithm assumes the first node to be fixed, the boundary conditions at the fixed end are readily met. The other constraints are met by estimating the corresponding reactions loads and treating these as external loads in the chain algorithm, and calculating the resulting deflections. In general, the error in the boundary conditions can then be calculated as

$$g_i(\mathbf{z}) = s_i(\mathbf{z}) - s_i^*; \quad i = 1, \ldots, n \tag{24}$$

where $g_i(\mathbf{z})$ is the boundary condition error (residual) function, $\mathbf{z}$ the reaction load vector, s_i^* the desired final value of s_i $(\mathbf{z})$, and n the number of boundary conditions. An iterative technique, or shooting method, is needed to solve the set of n nonlinear error functions. Two such methods, for example, are the Newton-Raphson technique and unconstrained optimization (Her, 1986). The Newton-Raphson technique finds a correction vector for $\mathbf{z}$, δ_z, by truncating the Taylor's series expansion of the error functions and evaluating the Jacobian matrix. The correction vector may then be found by

$$\begin{Bmatrix} \delta z_1 \\ . \\ . \\ . \\ \delta z_n \end{Bmatrix} = \begin{bmatrix} \frac{\partial g_1}{\partial z_1} & \frac{\partial g_1}{\partial z_2} & . & \frac{\partial g_1}{\partial z_n} \\ . & . & & . \\ . & . & & . \\ . & . & & . \\ \frac{\partial g_n}{\partial z_1} & \frac{\partial g_n}{\partial z_2} & . & \frac{\partial g_n}{\partial z_n} \end{bmatrix}_{\mathbf{z}}^{-1} \begin{Bmatrix} -g_1 \\ . \\ . \\ . \\ -g_n \end{Bmatrix}_{\mathbf{z}} \tag{25}$$

or

$$\{\delta z\} = [J]^{-1}\{-g\}$$

where $[J]^{-1}$ is the inverse of the Jacobian matrix. Since g_i cannot be expressed in closed form, the partial derivatives in $[J]$ must be evaluated numerically. The system of simultaneous linear equations in Eq. (25) may be solved by a method such as the Gaussian elimination method. Once the correction vector is found, a new reaction load vector is obtained as

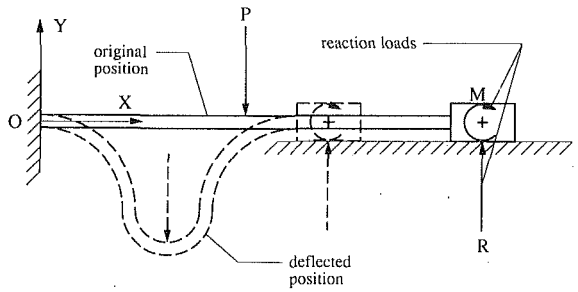

Fig. 7 Compliant slider mechanism and deflected configuration

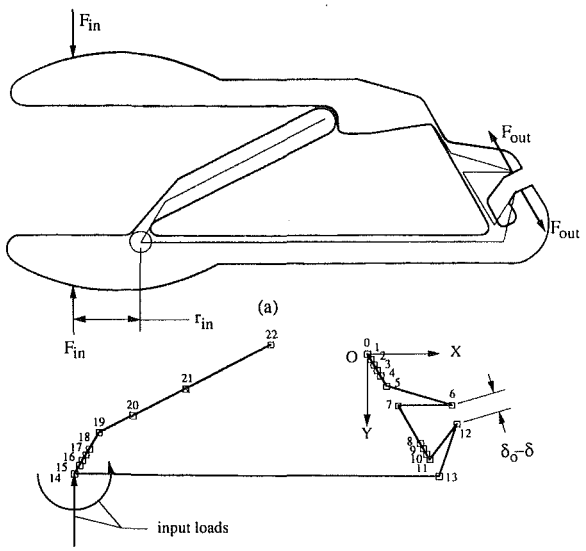

Fig. 8 Model for large-deflection calculations (*a*) compliant mechanism with outline of fully compliant model, and (*b*) discretization of model and boundary conditions

$$\{z\}^{new} = \{z\} + \{\delta z\} \tag{26}$$

This process is continued until the error (residual) functions are sufficiently close to zero.

An alternative to the use of the Newton-Raphson method is an unconstrained minimization algorithm, such as the Davidon-Fletcher-Powell method (Davidon, 1959; and Fletcher and Powell, 1963) or Powell's method (Powell, 1964). Such a method would be used to find the reaction loads, **z**, by minimizing the sum of the error functions squared, i.e.,

$$f(\mathbf{z}) = \sum_{i=1}^{n} [g_i(\mathbf{z})]^2 \tag{27}$$

The method has converged when the objective function, $f(\mathbf{z})$, is sufficiently close to zero.

Figure 8 shows the compliant hand tool [Fig. 8(*a*)] discretized into elements [Fig. 8(*b*)] and the associated boundary conditions. The main difference between the mechanism shown in Fig. 8(*a*) and that shown in Fig. 5(*c*) is the change in location of the passive pivot, as discussed previously, and aesthetic changes. Since the chain algorithm assumes node 0 to be fixed, the remaining boundary conditions will be met with the help of a shooting method. For instance, if no workpiece is placed in the output grips, then only the two boundary conditions at node 22 need be satisfied.

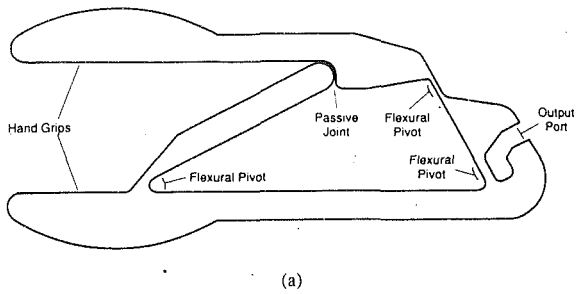

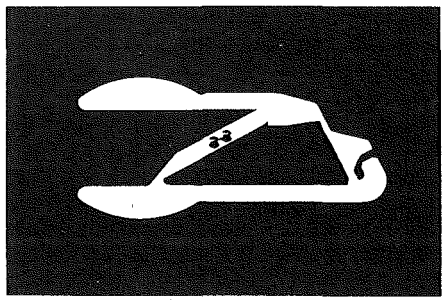

Fig. 9 (*a*) Final hand-tool design, and (*b*) photograph of finished product

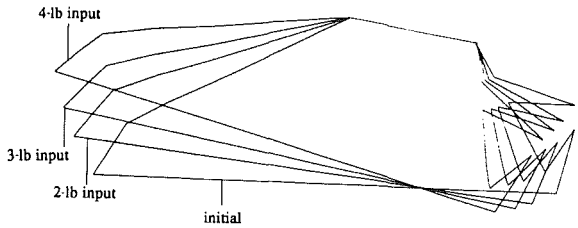

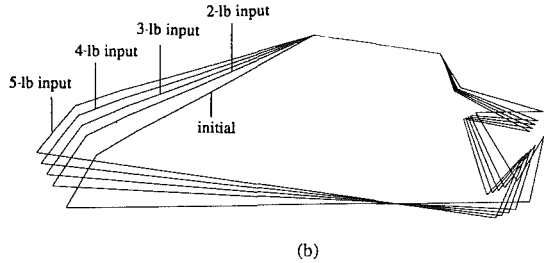

Fig. 10 (*a*) Mechanism deflection with no workpiece and (*b*) mechanism deflection with rigid workpiece

The final hand tool design is shown in Fig. 9(*a*) and a photograph of the finished product in Fig. 9(*b*). Its deformed configurations for different input loads and no workpiece is shown in Fig. 10(*a*). Figure 10(*b*) shows how the mechanism deforms under different input loads when gripping a rigid workpiece at the output port.

Performance Analysis. The fully compliant model is used to verify that the mechanism performs as desired and to improve the design as needed. This analysis is necessary for compliant mechanisms since the input/output characteristics are not easily calculated. For instance, the mechanical advantage of a compliant mechanism may vary as a function of the energy stored in the flexural pivots, the initial and final orientations, the method of loading, and the flexible and rigid segment dimensions.

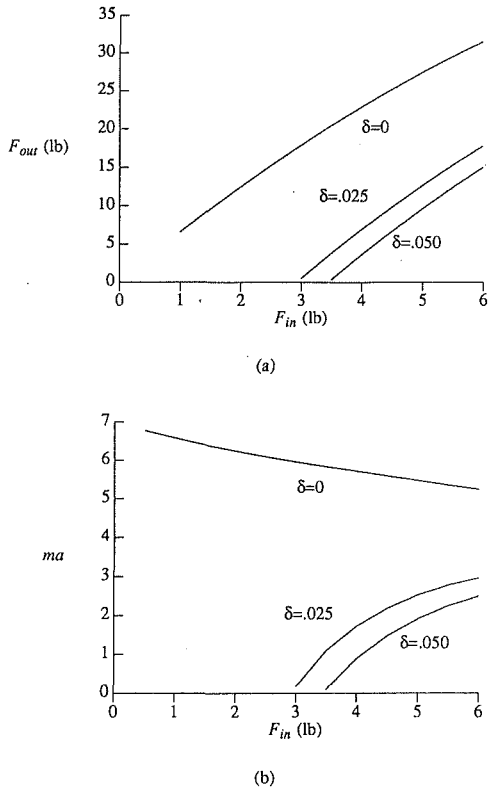

Fig. 11 Input/output characteristics of compliant hand-tool (*a*) output force versus input force, and (*b*) mechanical advantage versus input force, for various workpieces

Figures 11(a) and 11(b) show variations of the output force, F_{out}, the mechanical advantage, $ma = F_{out}/F_{in}$, respectively, with increasing input force, F_{in}, for the example design. The three graphs in each figure represent the effects of using different sized workpieces, where δ is the amount the output port deflects before gripping the workpiece, and δ_o is measured as the original undeflected distance between nodes 6 and 12 [Fig. 8(b)]. In comparison, a rigid-body mechanism working on a rigid workpiece would have a constant mechanical advantage with F_{in} for each given workpiece. The varying graphs for different workpieces illustrate the loss of energy to member deflection in compliant mechanisms. The increase in mechanical advantage, ma, [Fig. 11(b)] after initial contact with the workpiece, for $\delta = 0.025$ and $\delta = 0.050$, is due to the compliant mechanism's ability to deflect toward its toggle position.

Conclusion

The design methodology suggested and explained herein should prove to be useful in the design of compliant mechanisms, and offer an alternative to the trial and error methods currently used in industry. The pseudo-rigid-body model constitutes a powerful tool which allows the designer to use conventional knowledge of rigid-body mechanisms, and develop a significant portion of the design. The accuracy of the model increases as the lengths of the flexural pivots relative to those of the rigid sections decrease. This model is analyzed and modified to improve performance and satisfy design constraints. The modification and analysis procedure may be accomplished by simple iterative methods or formal optimization techniques. Once the pseudo-rigid-body analysis is completed, the mechanism performance is checked by using a fully compliant model, and the design can be further improved. This model involves a finite element formulation such as the chain algorithm and a shooting method. This model takes into account the geometric nonlinearities introduced by large deflections. The above methodology was demonstrated by the design of a one-piece hand tool. The hand tool served to exemplify the various stages of design, and also illustrated the combined effects of energy storage in flexural pivots, and the changing orientation approaching toggle.

Acknowledgment

The authors would like to acknowledge the School of Mechanical Engineering for the use of its facilities. The support of National Science Foundation, through NSF Grant No. MSS-8902777, is gratefully acknowledged. The first author would like to thank General Dynamics for their support through an educational leave of absence.

References

Bathe, K.-J., and Bolourch, S., 1979, "Large Displacement Analysis of Three-Dimensional Beam Structures," *International Journal for Numerical Methods in Engineering*, Vol. 14, pp. 961–986.

Bisshopp, K. E., and Drucker, D. C., 1945, "Large Deflections of Cantilever Beams," *Quarterly of Applied Mathematics*, Vol. 3, No. 3, pp. 272–275.

Burns, R. H., and Crossley, F. R. E., 1966, "Structural Permutations of Flexible Link Mechanisms," ASME Paper No. 66-MECH-5.

Davidon, W. C., 1959, "Variable Metric Method of Minimization," Argonne National Laboratory Report No. ANL-5990.

Erdman, A. G., and Sandor, G. N., 1984, *Mechanism Design: Analysis and Synthesis*, Vol. 1, Prentice-Hall, Inc., Englewood Cliffs, N.J.

Fletcher, R., and Powell, M. J. D., 1963, "A Rapidly Convergent Descent Method for Minimization," *Computer Journal*, Vol. 6, No. 2, pp. 163–168.

Frisch-Fay, R., 1962, *Flexible Bars*, Butterworth, Washington, D.C.

Gorski, W., 1976, "A Review of Literature and a Bibliography on Finite Elastic Deflections of Bars," *Transactions of the Institution of Engineers, Australia, Civil Engineering Transactions*, Vol. 18, No. 2, pp. 74–85.

Harrison, H. B., 1979, "Large Deformation Analysis of Submerged Ring Frames," *Journal of the Engineering Mechanics Division*, Proceedings of the ASCE, Vol. 105, No. EM5, pp. 829–837.

Her, I., 1986, "Methodology for Compliant Mechanism Design," Ph.D. Dissertation, Purdue University.

Her, I., and Midha, A., 1987, "A Compliance Number Concept for Compliant Mechanisms, and Type Synthesis," ASME JOURNAL OF MECHANISMS, TRANSMISSIONS, AND AUTOMATION IN DESIGN, Vol. 109,. No. 3, September, pp. 348–355.

Hill, T. C., 1987, "Applications in the Analysis and Design of Compliant Mechanisms," M.S. Thesis, Purdue University.

Midha, A., Her, I., and Salamon, B. A., 1992, "A Methodology for Compliant Mechanism Design: Part I—Introduction and Large-Deflection Analysis," *Advances in Design Automation*, ASME Book No. DE-Vol. 44-2, pp. 29–38.

Miller, R. E., 1980, "Numerical Analysis of a Generalized Plane Elastica," *International Journal for Numerical Methods in Engineering*, Vol. 15, pp. 325–332.

Paul, B., 1979, *Kinematics and Dynamics of Planar Machinery*, Prentice-Hall, Inc., Englewood Cliffs, New Jersey.

Powell, M. J. D., 1964, "An Efficient Method for Finding the Minimum of a Function of Several Variables Without Calculating Derivatives," *Computer Journal*, Vol. 7, No. 4, pp. 303–307.

Rao, S. S., 1984, *Optimization; Theory and Applications*, Wiley Eastern Limited, New Delhi.

Salamon, B. A., 1989, "Mechanical Advantage Aspects in Compliant Mechanisms Design," M.S. Thesis, Purdue University.

Sevak, N. M., and McLarnan, C. W., 1974, "Optimal Synthesis of Flexible Link Mechanisms with Large Static Deflections," ASME Paper No. 74-DET-83.

Shigley, J. E., and Mischke, C. R., 1989, *Mechanical Engineering Design*, Fifth Edition, McGraw-Hill Book Company, New York, New York.

Shoup, T. E., and McLarnan, C. W., 1971, "On the Use of Undulating Elastica for the Analysis of Flexible Link Mechanisms," ASME *Journal of Engineering for Industry*, Vol. 93, No. 1, pp. 263–267.

Shoup, T. E., 1972, "On the Use of the Nodal Elastica for the Analysis of Flexible Link Devices," ASME *Journal of Engineering for Industry*, Vol. 94, No. 3, pp. 871–875.

Timoshenko, S. P., and Gere, J. M., 1972, *Mechanics of Materials*, Litton Educational Publishing, Inc.

Vanderplaats, G. N., 1984, *Numerical Optimization Techniques for Engineering Design*, McGraw-Hill Book Company, New York.

Yang, T. Y., 1986, *Finite Element Structural Analysis*, Prentice-Hall, Inc., Englewood Cliffs, New Jersey.

Zienkiewicz, O. C., and Taylor, R. L., 1989, *The Finite Element Method*, McGraw-Hill Book Company, New York.

APPENDIX

Her (1989) proposed a finite element type algorithm for use in compliant mechanism analysis called the "chain algorithm."

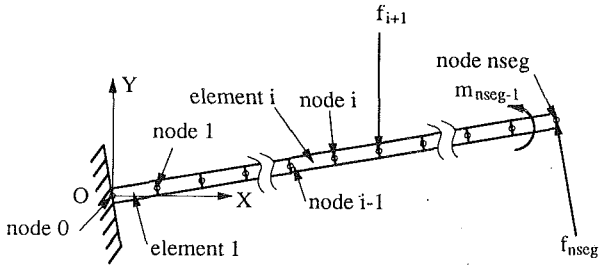

Fig. A1 Flexible cantilever beam discretized into nseg elements

Much of this work was developed from the earlier work by Harrison (1979) and Miller (1980). The chain algorithm is so named because it requires discretization of the object being modeled into beam elements and analyzes each element in succession. Each element is treated as a beam cantilevered at the end of the previous element. Equivalent loads are found for each cantilevered element, and its deflections are calculated.

To illustrate the procedure, consider a flexible cantilever beam (Fig. A1), discretized into a number of beam elements. The first node (node 0) is considered fixed and located at the origin of the global coordinate system O-X-Y. The deflection of element 1 is calculated by treating it as a cantilever beam, and loaded at node 1, as shown in Fig. A2(a). The end loads are the internal axial, transverse, and moment loads, calculated by use of the equations of static equilibrium, i.e.:

$$(P_{ax})_1 = \left[\sum_{i=1}^{n} (f_x)_i\right]\cos\theta_1 + \left[\sum_{i=1}^{n} (f_y)_i\right]\sin\theta_1$$

$$(P_{tr})_1 = -\left[\sum_{i=1}^{n} (f_x)_i\right]\sin\theta_1 + \left[\sum_{i=1}^{n} (f_y)_i\right]\cos\theta_1$$

$$M_1 = \sum_{i=1}^{n} m_i + \sum_{i=2}^{n} [(f_y)_i(x_i - x_1) - (f_x)_i(y_i - y_1)] \quad \text{(A1)}$$

where $(P_{ax})_1$, $(P_{tr})_1$ and M_1 are the internal axial load, transverse load, and moment at node 1, respectively, and $(f_x)_i$, $(f_y)_i$, and m_i are the externally applied loads in the global X and Y directions, and the externally applied moment at node i, respectively. These loads may now be used to calculate the deflections of the end of beam element 1:

$$\begin{pmatrix} \delta_{ax} \\ \delta_{tr} \\ \Delta\theta \end{pmatrix}_1 = [K]_1^{-1} \begin{pmatrix} P_{ax} \\ P_{tr} \\ M \end{pmatrix}_1 \quad \text{(A2)}$$

where $(\delta_{ax})_1$, $(\delta_{tr})_1$, and $\Delta\theta_1$ are the elastic axial, transverse and angular deflections, respectively, of element 1 at node 1 and $[K]_1^{-1}$ is the inverse of the stiffness matrix (flexibility matrix) for element 1. The axial deflection, δ_{ax}, is assumed to be negligible and the equations that follow reflect this assumption. The transverse deflection is easily transformed to global coordinates as follows:

$$\Delta X_1 = -(\delta_{tr})_1 \sin(\theta_1 + \Delta\theta_1)$$

$$\Delta Y_1 = (\delta_{tr})_1 \cos(\theta_1 + \Delta\theta_1) \quad \text{(A3)}$$

The new coordinates of node 1 are found as

$$x'_1 = x_1 + \Delta X_1$$

$$y'_1 = y_1 + \Delta Y_1 \quad \text{(A4)}$$

With the new coordinates of node 1 known, the deflection of element 2 can be found. To ensure compatibility between elements, element 2 and the remaining elements go through a rigid-body rotation such that the angular deflection at the end of element 1 is the same as that at the beginning of element 2. Element 2 is now considered to be cantilevered at node 1, internal loads are found and applied at node 3 and the corresponding deflections are found. This process is continued for each segment in the chain until the last element is reached. In general, the calculations for the ith element are similar to the special case of element 1, except for the changes in moment arm calculations in Eqs. (A1) and rigid-body rotations of earlier elements. This is illustrated in Fig. A2(b). The internal loads for the ith element can be written as

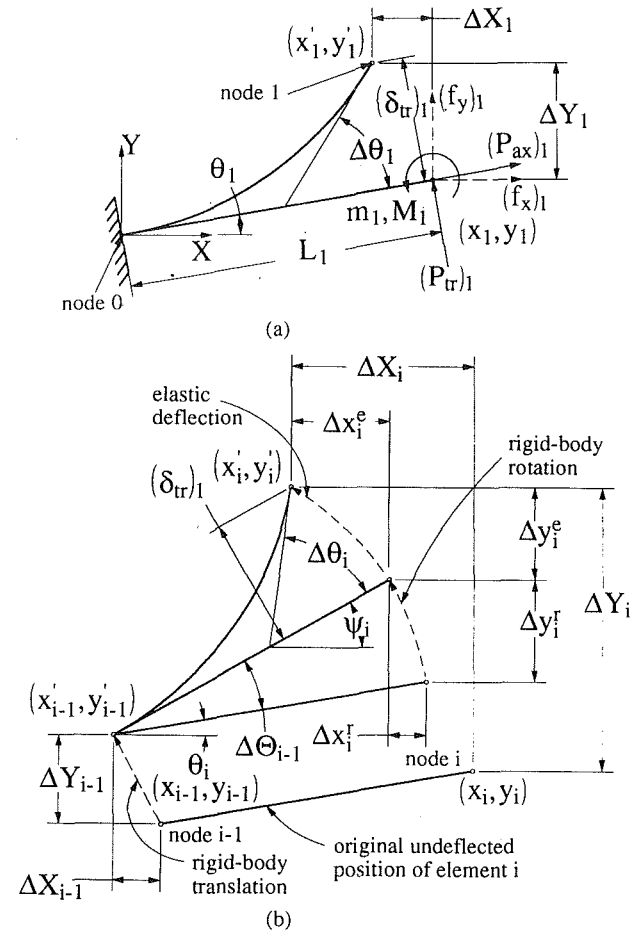

Fig. A2 (a) The deflection of element 1, and (b) the deflection of element i, as calculated by the chain algorithm

$$(P_{ax})_i = \left[\sum_{j=i}^{n} (f_x)_j\right]\cos\Psi_i + \left[\sum_{j=i}^{n} (f_y)_j\right]\sin\Psi_i$$

$$(P_{tr})_i = -\left[\sum_{j=i}^{n} (f_x)_j\right]\sin\Psi_i + \left[\sum_{j=i}^{n} (f_y)_j\right]\cos\Psi_i$$

$$M_i = \sum_{j=i}^{n} m_j + \sum_{j=i+1}^{n} [(f_y)_j \Delta\tilde{x}_{ji} - (f_x)_j \Delta\tilde{y}_{ji}] \quad \text{(A5)}$$

where

$$\Psi_i = \theta_i + \Delta\Theta_{i-1}$$

and $\Delta\Theta_{i-1}$ is the total angular displacement of the previous element; $\Delta\tilde{x}_{ji}$ and $\Delta\tilde{y}_{ji}$ are the distances from node i to node j using the most up-to-date coordinates (Salamon, 1989), and are defined as

$$\Delta\tilde{x}_{ji} = (x_j - x_i)\cos\Delta\Theta_{i-1} - (y_j - y_i)\sin\Delta\Theta_{i-1}$$

$$\Delta\tilde{y}_{ji} = (x_j - x_i)\sin\Delta\Theta_{i-1} + (y_j - y_i)\cos\Delta\Theta_{i-1} \quad \text{(A6)}$$

The deflection equations are similar in form to (A2):

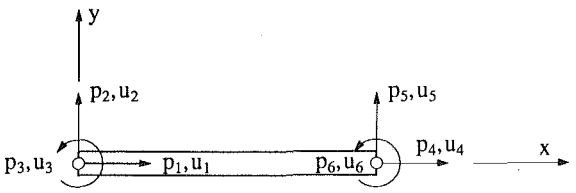

Fig. A3 Six-degree-of-freedom beam element

$$\begin{pmatrix}\delta_{ax}\\ \delta_{tr}\\ \Delta\theta\end{pmatrix}_i = [K]_i^{-1}\begin{pmatrix}P_{ax}\\ P_{tr}\\ M\end{pmatrix}_i \tag{A7}$$

The total displacements must now not only include the elastic displacements,

$$\Delta x_i^e = -(\delta_{tr})_i \sin\Psi_i$$
$$\Delta y_i^e = (\delta_{tr})_i \cos\Psi_i \tag{A8}$$

but also the rigid-body displacements caused by the angular deflections of the previous elements

$$\Delta x_i^r = L_i(\cos\Psi_i - \cos\theta_i)$$
$$\Delta y_i^r = L_i(\sin\Psi_i - \sin\theta_i) \tag{A9}$$

and the total x and y displacements of the previous elements. In other words:

$$\Delta X_i = \Delta X_{i-1} + \Delta x_i^r + \Delta x_i^e$$
$$\Delta Y_i = \Delta Y_{i-1} + \Delta y_i^r + \Delta y_i^e$$
$$\Delta\Theta_i = \Delta\Theta_{i-1} + \Delta\theta_i \tag{A10}$$

A considerable amount of error may be introduced into the formulation through inaccurate moment arm calculations in Eqs. (A5). This error stems from the fact that the calculations must be made from the latest available deflected positions rather than from the final deflected positions. This error can be reduced by using a load increment technique (Her, 1986) and iteration (Salamon, 1989).

The load increment technique works by applying the external load in increments. This means that some percentage of the load will be applied, the chain calculations performed, and the deflections found for this loading. The load is increased to the next percentage increment and the deflections are again calculated, only this time the moment arms are evaluated from the deflected position of the previous load increment calculations. The load increments can be written as:

$$(f_x^n)_i = \frac{n}{ninc}(f_x)_i$$
$$(f_y^n)_i = \frac{n}{ninc}(f_y)_i$$
$$m_i^n = \frac{n}{ninc} m_i$$
$$n = 1,2,\ldots, ninc \tag{A11}$$

where *ninc* is the number of load increments. The superscript n denotes the current load increment.

This method improves the accuracy of the chain calculations considerably, especially for relatively large deflections. As would be expected, the accuracy of the chain algorithm is increased with increasing number of load increments.

Iteration may be used with the load increment method to further improve accuracy. This is done by using the deflections found in the final load increment calculations to evaluate the new moment arms and new deflections for the full external load. This iteration may be continued until the desired accuracy is obtained.

The number of load increments and the number of iterations may be adjusted as needed to increase efficiency and accuracy. For instance, if a large number of load increments are used, then a small number of iterations at the end are needed, and vice versa.

The flexibility matrix $[K]_i^{-1}$ used in the beam deflection calculations of Eqs. (A7) may be found by considering the six-degree-of-freedom beam element shown in Fig. A3. The stiffness matrix for this element (Yang, 1986) may be written as:

$$\begin{pmatrix}p_1\\ p_2\\ p_3\\ p_4\\ p_5\\ p_6\end{pmatrix}_i = \frac{E_i}{L_i^3}\begin{bmatrix} AL^2 & 0 & 0 & -AL^2 & 0 & 0\\ 0 & 12I & 6IL & 0 & -12I & 6IL\\ 0 & 6IL & 4IL^2 & 0 & -6IL & 2IL^2\\ -AL^2 & 0 & 0 & AL^2 & 0 & 0\\ 0 & -12I & -6IL & 0 & 12I & -6IL\\ 0 & 6IL & 2IL^2 & 0 & -6IL & 4IL^2\end{bmatrix}_i$$
$$\times\begin{pmatrix}u_1\\ u_2\\ u_3\\ u_4\\ u_5\\ u_6\end{pmatrix}_i + \frac{(P_{ax})_i}{30L_i}\begin{bmatrix}0&0&0&0&0&0\\ 0&36&3L&0&-36&3L\\ 0&3L&4L^2&0&-3L&-L^2\\ 0&0&0&0&0&0\\ 0&-36&-3L&0&36&-3L\\ 0&3L&-L^2&0&-3L&4L^2\end{bmatrix}_i\begin{pmatrix}u_1\\ u_2\\ u_3\\ u_4\\ u_5\\ u_6\end{pmatrix}_i \tag{A12}$$

Using boundary conditions to reflect that each element in the chain algorithm is fixed to the previous element, i.e., $u_1 = u_2 = u_3 = 0$, the above matrix equation reduces to

$$\begin{pmatrix}P_{ax}\\ P_{tr}\\ M\end{pmatrix}_i = \left[\frac{E}{L^3}\begin{bmatrix}AL^2&0&0\\ 0&12I&-6IL\\ 0&-6IL&4IL^2\end{bmatrix} + \frac{P_{ax}}{30L}\begin{bmatrix}0&0&0\\ 0&36&-3L\\ 0&-3L&4L^2\end{bmatrix}\right]_i\begin{pmatrix}\delta_{ax}\\ \delta_{tr}\\ \Delta\theta\end{pmatrix}_i \tag{A13}$$

The flexibility matrix, $[K]_i^{-1}$, can be obtained by inverting the above stiffness (coefficient) matrix:

$$[K]_i^{-1} = \begin{bmatrix}\frac{L}{AE} & 0 & 0\\ 0 & \frac{4L^2Q_1 + 240EIL^3}{3(Q_2 + 240E^2I^2)} & \frac{LQ_1 + 120EIL^2}{Q_2 + 240E^2I^2}\\ 0 & \frac{LQ_1 + 120EIL^2}{Q_2 + 240E^2I^2} & \frac{12Q_1 + 240EIL}{Q_2 + 240E^2I^2}\end{bmatrix}_i \tag{A14}$$

where

$$(Q_1)_i = 2L_i^3(P_{ax})_i$$
$$(Q_2)_i = 3L_i^4(P_{ax})_i^2 + 140E_iI_iL_i^2(P_{ax})_i$$

An advantage of the flexibility matrix is that the deflection of each beam element is calculated individually, using the same equation. This eliminates the need to invert large stiffness matrices as required in conventional finite element analysis. As stated earlier, δ_{ax} in Eq. (A13) is assumed negligible.

The deflection equations can be simplified even further by alternatively defining an equivalent internal transverse load to approximate the nonlinear effects of axial stiffening (Timoshenko, 1941). The transverse load $(P_{tr})_i$ in Eqs. (A5) helps yield

$$(P_{tr})_{i,eq} = \frac{(P_{tr})_i}{1-\alpha_i} \tag{A15}$$

where

$$\alpha_i = \frac{(P_{ax})_i (2L_i)^2}{E_i I_i \pi^2}$$

The beam deflections can now be calculated using linear beam theory and the equivalent transverse load:

$$(\delta_{tr})_i = \frac{1}{E_i I_i}\left(\frac{(P_{tr})_{i,eq} L_i^3}{3} + \frac{M_i L_i^2}{2}\right)$$

$$\Delta\theta_i = \frac{1}{E_i I_i}\left(\frac{(P_{tr})_{i,eq} L_i^2}{2} + M_i L_i\right)$$

The error in these approximations increases with increasing axial force $(P_{ax})_i$.